This article has been accepted for publication in a future issue of this journal, but has not been fully edited. Content may change prior to final publication. Citation information: DOI 10.1109/JSEN.2018.2870255, IEEE Sensors Journal

CMOS Nanophotonic Sensor with Integrated Readout System

Abdul Shakoor, [1,2,*] Boon Chong Cheah, [1] Mohammed A. Al-Rawhani,[1] Marco Grande,[3] James Grant,[1] Luiz Gouveia, [1] David. R. S. Cumming, [1,*]

***Abstract*— The measurement of nanophotonic sensors currently requires the use of external measuring equipment for their read-out such as an optical spectrum analyser (OSA), spectrophotometer or detectors. This requirement of external laboratory based measuring equipment creates a "chip-in-a-lab" dilemma and hinders the use of nanophotonic sensors in practical applications. Making nanophotonic sensors usable in everyday life requires miniaturization of not only the sensor chip itself but also the equipment used for its measurement. In this paper, we have removed the need of external measuring equipment by monolithically integrating 1D grating structures with a complementary metal-oxide-semiconductor (CMOS) integrated circuit having an array of photodiodes. By doing so, we get a direct electrical read-out of the refractive index changes induced when applying different analytes to grating structures. The gratings are made of CMOS compatible silicon nitride. Employing a nanophotonic sensor made of CMOS compatible material allows fabrication of the integrated sensor chip in a commercial CMOS foundry, enabling mass production for commercialization with low cost. Our results present a significant step towards transforming present laboratory based nanophotonic sensors into practical portable devices to enable applications away from the analytical laboratory. We anticipate the work will have a major impact on technology for personalized medicine, environmental and industrial sensing.**

Index Terms— Diffraction gratings, Nanophotonics, Optoelectronics, Photodetectors, Sensors.

I. Introduction

Healthcare demands high performance sensor systems to ensure early diagnosis of diseases. The desirable performance parameters for a sensor system include high sensitivity, high detection limit [1], [2], low cost and compactness[3]. To meet the growing demands of high performance sensors, significant research effort has been invested to develop nanophotonic sensors. Over the last decade nanophotonic sensors have improved tremendously in terms of sensitivity and detection limit by using different sensor designs made of different materials[4]–[9]. Furthermore, the size of the nanophotonic sensor chips has reduced by exploiting different physical phenomena via various design configurations and compact integration of nanophotonic structures on the sensor chip[10]–[15]. However, while the nanophotonic sensor chips are small, their readout requires large and expensive laboratory-based equipment such as laser, spectrometer, optical spectrum analyzer (OSA) or detector. This requirement of laboratory-based equipment for the measurement of the nanophotonic sensor chips raises the "chip-in-a-lab" question, which means that although the size of the chip itself is small it requires laboratory-based equipment for its measurement. The "chip-in-a-lab" problem is therefore a major obstacle inhibiting the widespread deployment of nanophotonic sensors in everyday use for applications such as point-of-care diagnostics, security screening and environmental monitoring. Significant effort has gone into improving the performance parameters of the nanophotonic sensor chips themselves; however, there are only few reports on miniaturizing the whole sensor system [16]–[19]. For example, in reference[16], a compact nanophotonic sensor system is developed which uses a CMOS imager to measure fluorescence. However, this approach requires labelling of the bio-markers that negates one of the main advantages of nanophotonic sensors, i.e. label free sensing. Compact nanophotonic sensor systems capable to perform label-free sensing have been demonstrated in[17] but the sensor and the imaging chips are separate, requiring precise alignment and housing to hold the chips together, increasing complexity and system size. In 2010, Mazzotta et al integrated nanophotonic structures with bulk silicon photodiode (PD)[19] which made the size of the integrated chip large. Furthermore, the nanostructures are made of gold, which is incompatible with silicon device technology, hence not practical for mass production.

In this work, our approach towards developing a compact nanophotonic sensor system involves monolithic integration of resonant nanophotonic structures made of CMOS compatible material with a photodiode (PD) chip made using foundry

[1] School of Engineering, University of Glasgow, G12 8LT United Kingdom.
[2] Currently with Optoelectronics Research Center, University of Southampton, Highfield, Southampton, SO17 1BJ, United Kingdom
[3]Dipartimento di Ingegneria Elettrica e dell'Informazione, Politecnico di Bari, Bari 70125, Italy.
*Corresponding Author: shakabdul@gmail.com , david.cumming.2@glasgow.ac.uk

Funding for this work was provided by Physical Sciences Research Council (EPSRC), UK, grant No EP/K021966/1 , Fondo di Sviluppo e Coesione 2007-2013 – APQ Ricerca Regione Puglia "Programma regionale a sostegno della specializzazione intelligente e della sostenibilità sociale ed ambientale - FutureInResearch" (7K76VI3).

This article has been accepted for publication in a future issue of this journal, but has not been fully edited. Content may change prior to final publication. Citation information: DOI 10.1109/JSEN.2018.2870255, IEEE Sensors Journal

CMOS technology. The monolithically integrated compact nanophotonic sensor gives an electrical readout of the resonance wavelength shift of the resonant nanophotonic structures instead of measuring it by external detectors, OSA or spectrophotometer.

The schematic diagram, demonstrating the principle of operation of the resonant nanophotonic sensor integrated with the PD is shown in Figure 1.

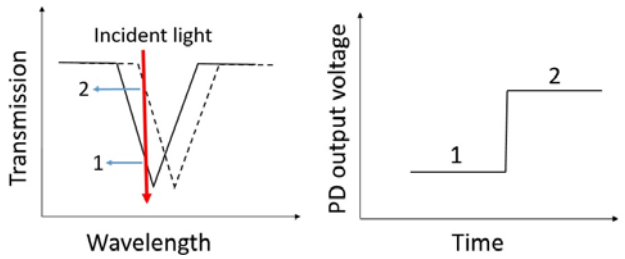

Figure 1: An illustration showing the principle of operation of the sensor system composed of resonant nanophotonic sensors monolithically integrated with a PD to obtain direct electrical read-out. The PD gives an output voltage level 1 for an input light source (red vertical bar). Introducing an analyte with higher refractive index red-shifts the resonance wavelength of the nanophotonic sensor. Keeping the intensity and wavelength of the input light source fixed with respect to the red vertical bar, the resonance wavelength shift of the nanophotonic sensors changes the intensity of light impinging on the integrated PD that is read-out as the change in the output voltage level of the PD (level 2).

The micro-electronics industry has been revolutionized by CMOS technology hence PDs made in CMOS are an excellent candidate for integration with nanophotonic sensors. The integration of nanophotonic sensors with PDs made in CMOS technology has the potential to enable the sensing industry to reap the combined benefits offered by CMOS technology and nanophotonics such as low cost, mass production, ease of integration with electronics and high sensing performance. For integration with CMOS technology, it is essential that the nanophotonic sensors are made of CMOS compatible material so that the complete integrated sensor can be fabricated in commercial CMOS foundries, enabling mass production and commercialization. For this reason, we have used a nanophotonic sensor made of silicon nitride (Si_3N_4) material for integration with the CMOS PD. Silicon nitride is fully CMOS compatible and has high transmission in the visible range where the absorption/sensitivity of a CMOS PD is high (500 – 750 nm). The nanophotonic sensors used in this work consist of 1D Si_3N_4 gratings that give a narrow resonance response in the visible region. A schematic of the integrated device is given in Figure 2.

II. Design, Fabrication and Packaging of the Sensor System

1D Si_3N_4 grating structures optimized for integration with CMOS detector chips were used as the sensor as they are simple structures possessing transmission characteristics such as resonance wavelength, linewidth, also known as full width at half maximum (FWHM), and a resonance depth that can easily be tuned according to requirements. Furthermore, they have reasonably high sensing performance, Si_3N_4 material is fully CMOS compatible and 1D-grating structures are straightforward to fabricate.

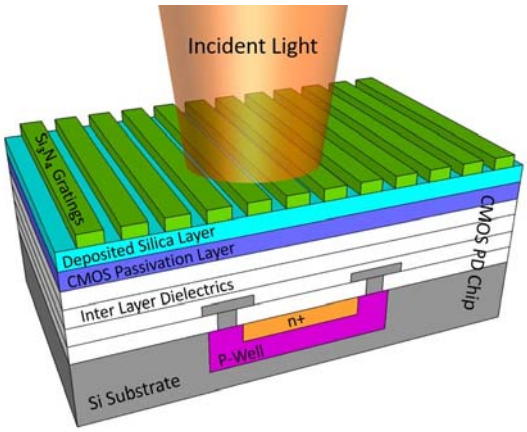

Figure 2: Schematic of the 1D grating structures integrated with the CMOS PD chip.

We started designing the gratings with the aim to achieve the minimum resonance wavelength at 600 nm to ensure that the resonance modes of the gratings overlap with the high sensitivity range of our CMOS detectors (500-750 nm). The corresponding periodicity of the gratings was then estimated using the formulation described in [20] which states that the effective refractive index of the i-th order mode should satisfy the following inequality in order to excite the guided mode in such grating structures:

$$max\{n_{sub}, n_{clad}\} \leq \left| n_{clad} \sin\theta_{inc} - i\frac{\lambda_o}{a} \right| \quad (1)$$

where n_{sub}, n_{clad} are the refractive indices of the substrate and the cladding of the gratings, respectively, θ_{inc} is the incidence angle, a the periodicity of gratings and λ_o is the guided mode resonance wavelength. In case $n_{sub} > n_{clad}$, equation 1 reduces to $\lambda_o = an_{sub}$ for the normal incidence condition. Using this equation the periodicity of the gratings was calculated as approximately 400 nm. The remaining physical parameters of the gratings such as thickness and the fill factor were optimized numerically by using a commercial software Rsoft (Diffract - MOD) which employs Rigorous Coupled Wave Analysis (RCWA).

The physical parameters and the characteristics of grating structures designed for this work are given in table 1.

Table 1: Physical parameters and characteristics of grating structures

Thickness	400 nm
Periodicity	400 nm
Fill factor	0.7
Operating wavelengths	400- 700 nm
Configuration	Normal incidence

This article has been accepted for publication in a future issue of this journal, but has not been fully edited. Content may change prior to final publication. Citation information: DOI 10.1109/JSEN.2018.2870255, IEEE Sensors Journal

The grating structures were designed to have a narrow resonance linewidth to achieve better sensitivity in terms of change in optical readout intensity on resonance wavelength shift, but not so narrow that it required a laser as an input light source. The resonance linewidth we typically measured from our grating structures was 8 nm, which would allow the use of an inexpensive light emitting diode (LED) as an input light source. Complete details of the grating design can be found in[21] along with the experimental transmission characteristics and the optical sensing performance where the measured optical sensitivity is reported to be 165 nm/RIU.

The CMOS detector chip was fabricated using a 0.35 µm high voltage foundry process from Austria Microsystems (AMS). The dimensions of the CMOS chip were only 3.5 x 3.5 mm and contained a 16 x 16 array of PDs, where each PD had dimensions of 6 x 8 µm. Some PDs on the chip were not covered by the grating structures in order to allow direct comparison between the performance of PDs with and without the nanophotonic structures.

For monolithic integration of the Si_3N_4 grating structures with the CMOS detector chip, a 500 nm layer of silica was first deposited, followed by a 400 nm layer of Si_3N_4, using a plasma enhanced chemical vapor deposition (PECVD) process. The top passivation layer of the CMOS detector chip made in the commercial foundry is usually composed of layers of different materials such as polyimide and silicon oxy-nitride. Since we do not have direct control of the foundry process that we access as a customer, the deposition of the 500 nm silica layer ensures that the lower cladding of Si_3N_4 gratings is silica. Ultimately both these layers could be integrated into the CMOS process flow. The grating structures were defined in the deposited 400 nm thick Si_3N_4 layer by e -beam lithography followed by dry etching. A 250 nm thick layer of a positive e-beam resist ZEP 520A was spin coated on the top nitride layer. The grating structures were defined in the resist by a 100 kV e-beam. The exposed areas were dissolved by o-xylene developer to create the mask for etching. The grating structures were then transferred to the Si_3N_4 layer by reactive ion etching using a CHF_3/O_2 gas chemistry. The resist mask was subsequently removed by 1165 remover followed by O_2 ashing.

Four identical Si_3N_4 grating arrays were fabricated on top of the CMOS PD chip, which appear as four darker squares in the microscopic image given in Figure 3a. The top right array is encircled in Figure 3a to highlight one of the array. The lighter area in between the grating arrays are PDs with no integrated gratings. The Si_3N_4 gratings on top of the CMOS chip were inspected using a scanning electron microscope (SEM) as depicted in Figure 3b. Inspecting the SEM images of the grating structures shows that the fabrication quality of gratings realized on the un-even top surface of the CMOS chip is comparable to the gratings fabricated on a flat glass slide reported in [21].

The CMOS chip with integrated Si_3N_4 gratings was attached to a chip carrier, wire-bonded and packaged using epoxy to protect the bond wires. A 3D printed ring made of Acrylonitrile-Butadiene-Styrene (ABS) was attached around the chip to enable experiments in aqueous solution by containing the liquid analyte over the chip surface.

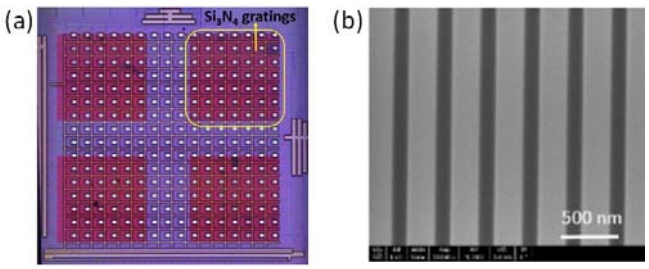

Figure 3: (a) Microscope image of the CMOS chip showing a 16x16 array of PDs. The four darker squares are Si_3N_4 gratings monolithically integrated on top of the CMOS PD chip. The top right array is encircled to highlight one of the grating arrays. The lighter areas in between the darker squares are PDs which are not covered with Si_3N_4 gratings. (b) SEM image of the Si_3N_4 gratings fabricated on top of the CMOS PD chip.

A compact printed circuit board (PCB) controlled by a LabVIEW programme was designed to carry out the sensing experiments. The LabVIEW programme was designed in such a way that the data from all the individual PDs on the CMOS chip could be extracted simultaneously from the same experimental run to enable comparison between the PDs with integrated gratings with those without gratings. The PCB was connected to a laptop computer via USB to obtain the electrical data. A picture of a complete sensor system including the read-out system is shown in Figure 4 which highlights the ease of use of the developed sensor. Here, we used a laptop computer but the system can easily be controlled by a tablet or smart phone using wireless technologies.

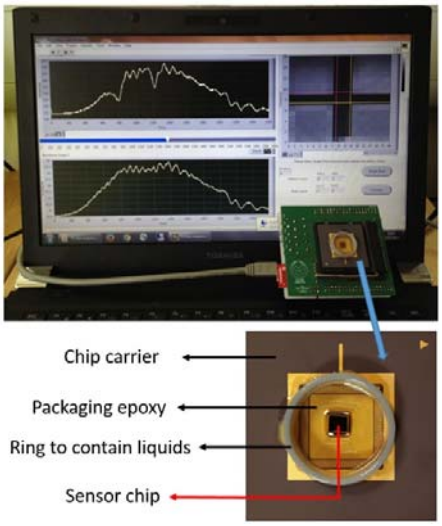

Figure 4: Packaged nanophotonic sensor with electrical readout system consisting of a PCB and computer giving an idea of the size and portability of the developed sensor. The lower part of the figure shows a magnified image of the packaged chip on a chip carrier.

III. Results and Discussion

The resonance wavelengths of the Si_3N_4 gratings integrated with the CMOS chip were determined by measuring the optical reflection spectrum of the gratings via photo-spectrometry. We used a commercial photo-spectrometry setup (Foster &

This article has been accepted for publication in a future issue of this journal, but has not been fully edited. Content may change prior to final publication. Citation information: DOI 10.1109/JSEN.2018.2870255, IEEE Sensors Journal

Freeman) that consists of a Leica 2700M microscope with an attached spectrometer. A polarizer was used to take reflection spectra in a transverse magnetic configuration (TM, the electrical field transverse to the gratings). The optical reflection spectrum shows two resonance peaks centered at 605 nm and 685 nm, as shown in Figure 5. The optical reflection spectrum consists of Fabry - Perot fringes that arise because of the back reflections from the multiple layers of the CMOS chip that are made of different materials, as depicted in the cross-section of the chip given in Figure 2.

The electrical spectrum of the gratings integrated with the CMOS detectors was measured to identify the resonance wavelengths of the gratings in the electrical read-out from the PDs. Although, the optical reflection spectrum shown in Figure 5 allows identification of the resonance wavelength positions of the gratings, it is important to measure the position of the resonance wavelengths in the electrical measurements because the measured electrical spectrum in our system is a convolution of the grating transmission characteristics, monochromator output intensity and the PD quantum efficiency that will shift the measured resonance wavelengths of the gratings compared to those achieved in the reflection mode optical spectrum.

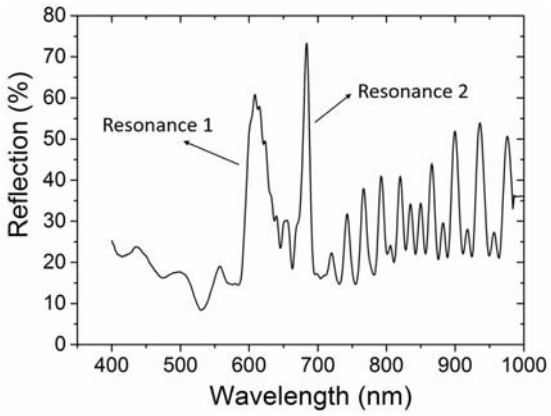

Figure 5: Optical reflection spectrum of the Si_3N_4 gratings integrated with the CMOS PD chip with air cladding.

To obtain the electrical transmission spectrum of the gratings integrated with the CMOS PD, the wavelength of the incident light was scanned from 400 to 1000 nm using a monochromator with a halogen lamp as the light source. The measured linewidth of the incident light was 4 nm. The light transmitted through the gratings and detected by the PD was read out as an output voltage that gives a transmission spectrum of the gratings in units of voltage.

The output voltage of the PD with integrated gratings for different wavelengths of incident light is shown in Figure 6 (black curve). The output voltage spectrum of the PD with integrated gratings shows two clear dips at 595 nm and 675 nm that correspond to the two resonance positions of the gratings that were observed in the optical reflection-mode spectrum. These dips are not present in the output voltage curve of the PD with no integrated gratings, as shown in Figure 6 (red curve), confirming that the appearance of the dips arise from the resonance response of the grating.

It was observed that the dark signal of the PDs (PD output voltage with no incident light) with integrated gratings is higher compared to the unprocessed PDs on the same chip. The increase in the dark signal may be due to the high voltage e-beam involved during the fabrication of the gratings on top of the CMOS chip. For better comparison, the output voltage level of the spectrum of the PD without integrated gratings is normalized to the same level as that of the PD with integrated gratings in Figure 6.

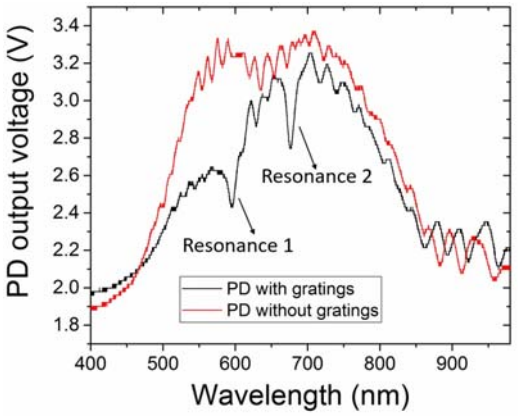

Figure 6: Comparison between the output voltage spectra of the PD with (black curve) and without (red curve) integrated gratings. Two dips in the electrical spectrum of the PD with integrated gratings corresponds to the resonance wavelengths of the grating structures which are absent in the electrical spectrum of the PD with no gratings. The two spectra have different dark signal levels (output current or voltage with no incident light) and hence the output voltage level of the PD without integrated gratings has been normalized to match the output voltage level of the PD with gratings to make the comparison clearer. These spectra are taken with air cladding.

To evaluate the sensing performance of the integrated sensor different concentrations of glycerol solution diluted in DI water were added on top of the sensor. Increasing the concentration of glycerol in DI water increases the refractive index[22]. Introducing higher concentrations of glycerol shows a red-shift of the resonance in the electrical spectrum as shown in the Figure 7a. By fixing the wavelength of the input light, the sensitivity response of the integrated sensing system can be evaluated from Figure 7a. using the method illustrated in Figure 1. From Figure 7a, it can be seen that the maximum sensitivity in terms of change in the output voltage owing to the resonance wavelength shift on introducing an analyte is achieved if the input wavelength is fixed at 618 nm. This wavelength corresponds to the maximum slope of the resonance dip. By keeping the input wavelength fixed at 618 nm and analysing the response shown in Figure 7a, the sensitivity curve is extracted which is shown in Figure 7b.

It is observed that there is a negligible change in the PD output voltage for an initial increase in glycerol concentrations (0 % to 20 %) as the optical intensity detected by the PD, which, as previously noted, is the convolution of the input light at 618 nm and the resonance response of the grating, stays almost at the same level. On the other hand, for higher concentrations the optical intensity detected by the PD increases leading to a

This article has been accepted for publication in a future issue of this journal, but has not been fully edited. Content may change prior to final publication. Citation information: DOI 10.1109/JSEN.2018.2870255, IEEE Sensors Journal

higher PD output voltage. Please note that the lack of signal change for 0-20% glycerol concentrations is only due to the selection of the input wavelength. As the designed gratings have narrow line width, the signal saturates for a large change in the refractive index. In fact, the gratings are designed to sense small changes in the refractive index with high sensitivity. Depending on the properties of the analyte, the input wavelength can be adjusted to maximize the performance of the device for a particular analyte. From Figure 7b, we evaluated the sensitivity of the integrated sensing system to be equal to 6.5 V/RIU, which means that for a RIU change, the change in the output electrical signal is 6.5 V. The measured sensitivity value is higher than our previous work on monolithic integration of plasmonic sensors with CMOS PDs[23], [24]. The improvement of sensitivity is due to the narrower resonance linewidth of the gratings structures compared to the plasmonic structures. Please note that the sensitivity value we report here also depend on the electronic readout circuitry and can vary based on the design of readout electronics.

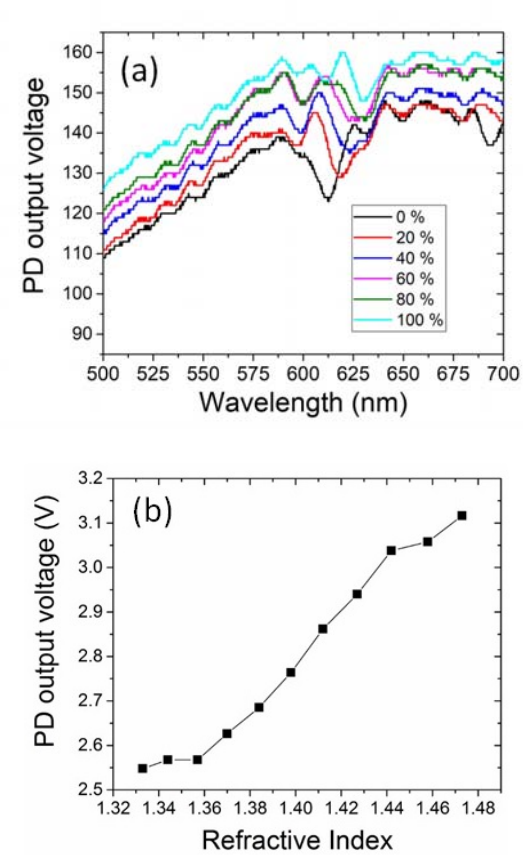

Figure 7a: (a) Shift of the resonance wavelength in the electrical spectrum of the gratings on application of different concentrations of glycerol (b) sensitivity analysis (change in the output voltage of the PD) curve based on the electrical spectrum shift for 618 nm incident light.

The second approach to evaluate the sensor performance is to directly measure the change in the output voltage of the PD at one input wavelength caused by introducing analytes having different refractive indices (different concentrations of glycerol in our experiments) instead of scanning the input wavelength. As before, for initial concentrations of glycerol a negligible change in the output voltage is observed while for higher concentrations the output voltage change is large (0.098 V) as shown in Figure 8. This is consistent with the results shown in Figure 7b. The non-linearity in the sensing response of the grating structures is due to its narrow band resonance response.

The 0.098 V change in voltage occurs due to 0.015 change in refractive index. Our sensor system can measure a minimum voltage change of 0.0198 V, i.e. five times lower than that measured for 0.015 refractive index change. Hence, the sensor system has a detection limit of 0.003 RIU, which is an order of magnitude better than our previous work[23]. However, working at the resolution limit of the detector induces error factors since the noise associated with electronic read-out becomes significant. The detection limit is lower compared to resonant nanophotonic sensors measured by external specialized equipment such as OSA or spectrometer. This is because in our integrated system nanophotonic structures are integrated with PDs made by CMOS technology, which consists of thick passivation layer and multiple inter-layer dielectrics, that induces back reflections and a lose of optical signal. The performance of our integrated nanophotonic sensor can be improved by etching away the passivation layer, which in addition to reducing the back-reflections will also shorten the gap between the nanophotonic structures and the PDs. The performance can be further enhanced by improvements in the electronic readout circuitry. The measured sensitivity using this approach is also 6.5 V/RIU, which is equal to the sensitivity value extracted from the shift of the electrical transmission spectrum shown in Figure 7.

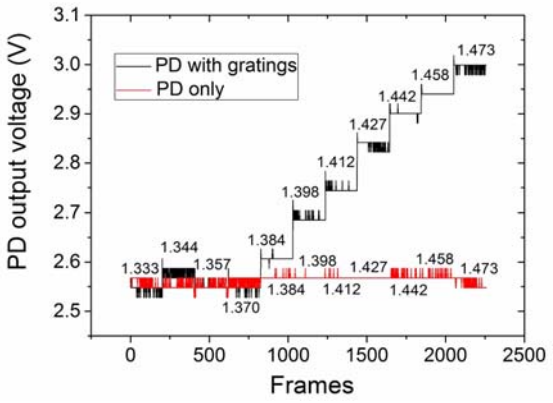

Figure 8: Increase in the PD output voltage due to the change in the resonance wavelength of the grating structures integrated with the CMOS PD on application of different concentrations of glycerol corresponding to different refractive indices. As a control measurement, the output voltage of the PD without integrated gratings is also given and does not show any change in the output voltage when different concentrations of glycerol are applied.

As a control measurement, Figure 8 also shows the output voltage of the PD that does not have gratings integrated on top of it. The curves shown in Figure 8 are obtained simultaneously from the same chip and experimental run. There is no change in the output voltage of the PD with no gratings integrated on it when different concentrations of glycerol are applied which clearly shows that the increase of the PD output voltage having integrated gratings is due to the resonance wavelength shift of the gratings. The control measurement is also used to monitor the intensity fluctuations of the incident light source, which is

stable in the time frame of the measurements (2200 frames corresponding to 3 minutes) as shown in the Figure 8. The stability of the system was checked by running the measurement for single refractive index condition for one hour. The PD output voltage was found to be stable throughout this period (not shown here). This work can be extended to perform biological assays as the nanophotonic sensors are made of silicon nitride which can be functionalized for a range of biosensing experiments[25], [26].

IV. CONCLUSION

We have demonstrated a miniaturized nanophotonic sensor system implemented monolithically by integration of nanophotonic structures with CMOS PDs. By doing so, the need of external laboratory based equipment for measurement of nanophotonic sensors is eliminated ,overcoming the well-known "chip-in-a-lab" problem. The developed nanophotonic sensor system gives direct electrical readout of the refractive index changes of the environment surrounding the nanophotonic sensors through PDs integrated monolithically with the nanophotonic sensors. By careful selection of the input wavelength, an electrical sensitivity value of 6.5 V/RIU is obtained. . The nanophotonic sensor is made of Si_3N_4 that is fully CMOS compatible, allowing fabrication of the entire integrated sensing chip in commercial foundries, which would lead to cheap mass production and ease of commercialization. The off-chip optics does not rely on an expensive laser and could be reduced to a simple LED. By incorporating microfluidic channels, the capability of the developed sensor can be extended to carryout multiple assays on the single chip simultaneously by utilizing an array of PDs on the same CMOS chip. This work is a step forward towards making the use of nanophotonic sensors practical in many applications, especially in point-of-care diagnostics.

ACKNOWLEDGMENT

We thank technical staff of James Watt Nanofabrication Center (JWNC) at university of Glasgow for their support in device fabrication. The data set for this work can be accessed by following DOI: 10.5525/gla.researchdata.432

REFERENCES

[1] I. M. White and X. Fan, "On the performance quantification of resonant refractive index sensors," *Optics Express*, vol. 16, no. 2, p. 1020, 2008.

[2] L. Guo, J. A. Jackman, H. H. Yang, P. Chen, N. J. Cho, and D. H. Kim, "Strategies for enhancing the sensitivity of plasmonic nanosensors," *Nano Today*, vol. 10, no. 2, pp. 213–239, 2015.

[3] D. Y. Fedyanin and Y. V Stebunov, "All-nanophotonic NEMS biosensor on a chip.," *Scientific reports*, vol. 5, p. 10968, 2015.

[4] C. Valsecchi and A. G. Brolo, "Periodic metallic nanostructures as plasmonic chemical sensors," *Langmuir*, vol. 29, no. 19, pp. 5638–5649, 2013.

[5] J. N. Anker, W. P. Hall, O. Lyandres, N. C. Shah, J. Zhao, and R. P. Van Duyne, "Biosensing with plasmonic nanosensors.," *Nature materials*, vol. 7, no. 6, pp. 442–453, 2008.

[6] M. E. Stewart *et al.*, "Nanostructured plasmonic sensors," *Chemical Reviews*, vol. 108, no. 2, pp. 494–521, 2008.

[7] E. Melnik *et al.*, "Local functionalization of CMOS-compatible Si3N4 Mach-Zehnder interferometers with printable functional polymers," *Sensors and Actuators B: Chemical*, vol. 236, pp. 1061–1068, 2016.

[8] D. F. Dorfner, T. Hürlimann, T. Zabel, L. H. Frandsen, G. Abstreiter, and J. J. Finley, "Silicon photonic crystal nanostructures for refractive index sensing," *Applied Physics Letters*, vol. 93, no. 18, pp. 2006–2009, 2008.

[9] A. Di Falco, L. O'Faolain, and T. F. Krauss, "Chemical sensing in slotted photonic crystal heterostructure cavities," *Applied Physics Letters*, vol. 94, no. 6, pp. 93–96, 2009.

[10] J. Wang, Z. Yao, and A. W. Poon, "Silicon-Nitride-Based Integrated Optofluidic Biochemical Sensors Using a Coupled-Resonator Optical Waveguide," *Frontiers in Materials*, vol. 2, no. April, pp. 1–13, 2015.

[11] M. G. Scullion, A. Di Falco, and T. F. Krauss, "Slotted photonic crystal cavities with integrated microfluidics for biosensing applications," *Biosensors and Bioelectronics*, vol. 27, no. 1, pp. 101–105, 2011.

[12] Y. Sun and X. Fan, "Optical ring resonators for biochemical and chemical sensing," *Analytical and Bioanalytical Chemistry*, vol. 399, no. 1, pp. 205–211, 2011.

[13] F. Vollmer, L. Yang, and S. Fainman, "Label-free detection with high-Q microcavities: A review of biosensing mechanisms for integrated devices," *Nanophotonics*, vol. 1, no. 3–4, pp. 267–291, 2012.

[14] P. Muellner, E. Melnik, G. Koppitsch, J. Kraft, F. Schrank, and R. Hainberger, "CMOS-compatible Si3N4 waveguides for optical biosensing," *Procedia Engineering*, vol. 120, pp. 578–581, 2015.

[15] C. A. Barrios, "Optical slot-waveguide based biochemical sensors," *Sensors (Switzerland)*, vol. 9, no. 6, pp. 4751–4765, 2009.

[16] L. Hong, S. McManus, H. Yang, and K. Sengupta, "A fully integrated CMOS fluorescence biosensor with on-chip nanophotonic filter," *IEEE Symposium on VLSI Circuits, Digest of Technical Papers*, vol. 2015–Augus, pp. C206–C207, 2015.

[17] A. E. Cetin *et al.*, "Handheld high-throughput plasmonic biosensor using computational on-chip imaging," *Light: Science & Applications*, vol. 3, no. 1, p. e122, 2014.

[18] G. J. Triggs, Y. Wang, C. P. Reardon, M. Fischer, G. J. O. Evans, and T. F. Krauss, "Chirped guided-mode resonance biosensor," *Optica*, vol. 4, no. 2, pp. 1–6, 2017.

[19] F. Mazzotta, G. Wang, C. Hägglund, F. Höök, and M. P. Jonsson, "Nanoplasmonic biosensing with on-chip electrical detection," *Biosensors and Bioelectronics*, vol. 26, no. 4, pp. 1131–1136, 2010.

[20] S. S. Wang and R. Magnusson, "Theory and applications of guided-mode resonance filters.," *Applied optics*, vol. 32, no. 14, pp. 2606–2613, 1993.

[21] A. Shakoor, M. Grande, J. Grant, and D. R. S. Cumming, "One-Dimensional Silicon Nitride Grating Refractive Index Sensor Suitable for Integration with CMOS

Detectors," *IEEE Photonics Journal*, vol. 9, no. 1, 2017.
[22] L. F. Hoyt, "New Table of the Refractive Index of Pure Glycerol at 20°C," *Industrial & Engineering Chemistry*, vol. 26, no. 3, pp. 329–332, 1934.
[23] A. Shakoor *et al.*, "Plasmonic Sensor Monolithically Integrated with a CMOS Photodiode," *ACS Photonics*, vol. 3, no. 10, pp. 1926–1933, 2016.
[24] A. Shakoor *et al.*, "Monolithic integration of a plasmonic sensor with CMOS technology," vol. 10107, p. 101070F, 2017.
[25] A. Arafat *et al.*, "Covalent Biofunctionalization of Silicon Nitride Surfaces," no. 28, pp. 6233–6244, 2007.
[26] G. Pezzotti *et al.*, "Bioactive silicon nitride : A new therapeutic material for osteoarthropathy," *Nature Publishing Group*, no. September 2016, pp. 1–11, 2017.